



# Structural modification and band gap engineering of sol–gel dip-coated thin films of $\text{Zn}_{0.75}\text{Mg}_{0.25}\text{O}$ alloy under vacuum annealing

NRIPASREE NARAYANAN and N K DEEPAK\*

Department of Physics, Kannur University, Kannur 670 327, India

\*Corresponding author. E-mail: dr.deepaknk@yahoo.com

MS received 28 October 2015; revised 1 February 2016; accepted 17 March 2016; published online 3 November 2016

**Abstract.** In the present study, we investigated the effect of vacuum annealing on the structural and optical properties of sol–gel dip-coated thin films of  $\text{Zn}_{0.75}\text{Mg}_{0.25}\text{O}$  alloy. XRD studies revealed that all these films were polycrystalline with hexagonal wurtzite structure and there was no trace of additional phases other than ZnO. With increase in annealing temperature, the samples showed preferred orientation along the  $c$ -axis, (0 0 2) plane and also peak narrowing and peak shift towards higher angles. The calculated values of mean crystallite size increased with annealing temperature indicating the improvement in crystallinity. Heat treatment caused lattice contraction and a decrease in film thickness. The optical transmittance in the visible spectral range enhanced with increase in annealing temperature while the fundamental absorption edge in the near ultra-violet region got red-shifted with annealing. The calculated values of optical energy gap of the samples showed a decrease with heat treatment due to the improvement in crystallinity during annealing and hence the subsequent decrease in quantum size effect.

**Keywords.**  $\text{Zn}_{0.75}\text{Mg}_{0.25}\text{O}$ ; sol–gel dip coating; vacuum annealing; red-shift.

**PACS Nos** 81.05.Bx; 61.05.cp; 81.40.Tv

## 1. Introduction

Zinc oxide (ZnO) thin films are very promising candidates in the field of optoelectronics. Being a semiconductor with large optical energy gap, it belongs to a unique class of materials called transparent conducting oxides. ZnO also possesses large free exciton binding energy of 60 meV leading to efficient exciton emission at room temperature. In addition, it is a low-cost, non-toxic and biocompatible material with good thermal and chemical stabilities. These unique properties of ZnO thin films make it suitable for applications in solar cells [1], photodetectors [2], light emitting diodes [3], thin film transistors [4], gas sensors [5] etc.

Zinc oxide has a direct optical energy gap of 3.37 eV at room temperature so that the fundamental absorption occurs in the near-ultraviolet region. The band-gap energy can be tailored by alloying with materials such as MgO, CdO etc. which have different band gaps [6]. By alloying with MgO, we shall get larger band

gap while alloying with CdO results in a red-shift in the energy gap value. Ohtomo *et al* [7] were the first, to prepare  $\text{Zn}_{1-x}\text{Mg}_x\text{O}$  by pulsed laser deposition and obtain a maximum band gap of 4.15 eV. Lin *et al* [8] reported a study based on Mg-doped ZnO films using sol–gel deposition technique and attained a band gap of 3.4 eV. Matsubara *et al* [9] prepared aluminium-doped  $\text{Zn}_{1-x}\text{Mg}_x\text{O}$  films by pulsed laser deposition. Misra *et al* [10] successfully deposited  $\text{Zn}_{1-x}\text{Ca}_x\text{O}$  by sol–gel method and obtained a maximum band gap energy of 3.81 eV.

In the literature, many techniques such as atomic layer deposition [11], sputtering [12], spray pyrolysis [13], sol–gel spin coating [14], sol–gel dip coating [15], chemical vapour deposition [16], pulsed laser deposition [17] etc. have been reported for the successful deposition of ZnO thin films. In this work, a simplified low-cost sol–gel dip coating was adopted for the deposition of  $\text{Zn}_{0.75}\text{Mg}_{0.25}\text{O}$  thin films and the influence of vacuum annealing on the structural and optical properties of these films was studied.

## 2. Experimental methods

$\text{Zn}_{0.75}\text{Mg}_{0.25}\text{O}$  thin films were deposited on glass substrates by sol–gel dip coating method. Zinc acetate dihydrate  $[\text{Zn}(\text{CH}_3\text{COO})_2 \cdot 2\text{H}_2\text{O}]$  and magnesium acetate tetrahydrate  $[\text{Mg}(\text{CH}_3\text{COO})_2 \cdot 4\text{H}_2\text{O}]$  were used as the precursor and dopant respectively while 2-methoxy ethanol and monoethanolamine (MEA) were taken as the solvent and stabilizer respectively. Appropriate quantities of zinc acetate dihydrate and magnesium acetate tetrahydrate were first dissolved in a mixture of 2-methoxyethanol and MEA. Throughout the experiment, the molarity of the precursor solution was kept fixed at 0.5 M and the molar ratio of MEA to zinc acetate was kept at 1.0. The prepared solutions were then stirred at  $70^\circ\text{C}$  for 1 h with a hot magnetic stirrer to yield a clear homogeneous solution and were then aged for 24 h at room temperature.

The aged solutions were then deposited on pre-cleaned glass substrates by using Holmarc Dip Coating unit (HO-TH-01). Film deposition was carried out in air at room temperature with a controlled dipping and withdrawal speed of 50 mm/min. Every time the substrate was withdrawn from the solution, the film was allowed to dry and subjected to a pre-heat treatment at  $250^\circ\text{C}$  in a hot air oven. This procedure was repeated five times. As the final step, the film was subjected to post-heat treatment at  $300^\circ\text{C}$  for 15 min in an electric furnace. The as-prepared samples were then annealed at  $100\text{--}400^\circ\text{C}$  for 3 h in a high vacuum of  $10^{-5}$  mbar. Even though we tried to prepare  $\text{Zn}_{0.75}\text{Mg}_{0.25}\text{O}$  thin films, there will be a possible deviation from this particular stoichiometry and here we had not performed any composition analysis to determine the exact stoichiometry.

The prepared films were then subjected to X-ray diffraction (XRD) studies for structural characterization using X-ray Diffractometer (Bruker AXS D8 Advance) with  $\text{CuK}\alpha$  radiation ( $\lambda = 1.5046 \text{ \AA}$ ) at 40 kV and 35 mA in the scanning angle ( $2\theta$ ) ranging from  $5^\circ$  to  $75^\circ$  with a scan speed of  $0.001^\circ/\text{min}$ . Optical studies were carried out using Jasco V-650 UV–Vis Spectrophotometer in the  $300\text{--}900 \text{ nm}$  wavelength range.

## 3. Results and discussion

### 3.1 Structural studies

The XRD patterns of the unannealed and vacuum-annealed samples of  $\text{Zn}_{0.75}\text{Mg}_{0.25}\text{O}$  thin films are presented in figure 1. All the films were polycrystalline

in nature with hexagonal wurtzite structure. As there is no additional phase corresponding to  $\text{MgO}$ , we can confirm the monophasic nature of the as-deposited and vacuum-annealed films of  $\text{Zn}_{0.75}\text{Mg}_{0.25}\text{O}$  alloy. This can be due to the successful incorporation of  $\text{Mg}^{2+}$  ions either at the  $\text{Zn}^{2+}$  lattice site or at interstitial positions. All the films showed preferential orientation along the  $c$ -axis (0 0 2) plane. But at higher annealing temperatures, the films showed a tendency to grow along (1 0 0) and (1 0 1) planes also. This might be attributed to the increase of growth rate along these planes because during annealing, thermal energy is available for the activation of growth along these directions also.

A detailed analysis of the XRD pattern showed a slight shift of the diffraction angle  $2\theta$  corresponding to the (0 0 2) peak towards higher values. Usually, peak shift indicates a change in lattice parameters as well as variation in chemical composition. During thermal annealing, the defects and disorders will be removed from the lattice site and hence the lattice suffers a contraction. As a result, we observed peak shift towards higher angle values in the diffractograph. Figure 2 shows the variation of peak position and full-width at half-maximum (FWHM) intensity of (0 0 2) peak as a function of annealing temperature. The peaks showed a decrease in FWHM values with increase in annealing temperature. In XRD, the peak broadening is mainly dependent on the diffracting crystalline size. Thus, the

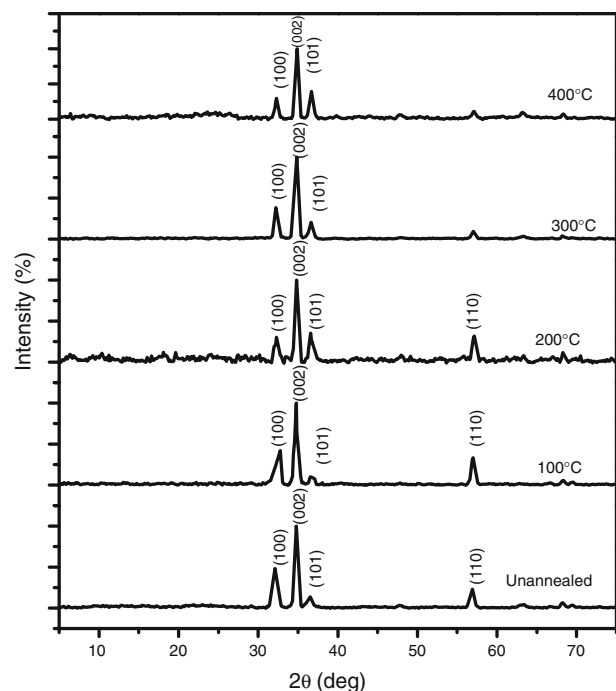


**Figure 1.** XRD profile of unannealed and vacuum-annealed samples of  $\text{Zn}_{0.75}\text{Mg}_{0.25}\text{O}$  thin films.

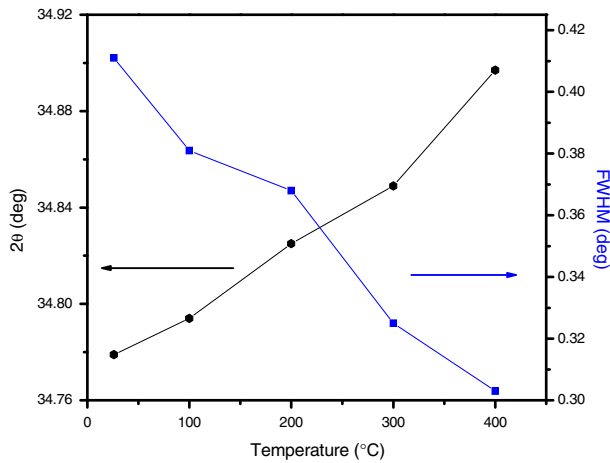


**Figure 2.** Variation of peak position ( $2\theta$ ) and FWHM with annealing temperature.

**Table 1.** Variation of peak position ( $2\theta$ ), FWHM ( $\beta$ ) and mean crystallite size for the unannealed and annealed samples.

Temperature (°C)	$2\theta$ (°)	$\beta$ (°)	$D$ (nm)
Unannealed	34.779	0.411	21.25
100	34.794	0.381	21.85
200	34.825	0.368	22.62
300	34.849	0.325	25.62
400	34.897	0.303	27.48

observed peak narrowing in the present case implies the improvement in crystallinity with annealing as it accelerates the merging process [18]. In polycrystalline ZnO thin films, there are large numbers of dangling bonds at the grain boundaries arising from zinc or oxygen deficiencies. When sufficient thermal energy is available during annealing, these dangling bonds favour merging of smaller crystallites to form larger ones. The mean crystallite size of the prepared samples was calculated using the Scherrer formula [19]

$$D = \frac{0.9\lambda}{\beta \cos \theta}, \quad (1)$$

where 0.9 is the value of the shape factor,  $\lambda$  ( $=1.5406 \text{ \AA}$ ) is the wavelength of the X-rays used,  $\beta$  is the full-width at half-maximum intensity in radians and  $\theta$  is the Bragg's angle.

The calculated values of mean crystallite size for (002) peak are presented in table 1. All the films possessed nanostructured crystallites and the size increased with increase in annealing temperature. Thus, vacuum annealing improved the crystallinity of the thin films. The formation of thin films generally involves nuclei formation, growth and coalescence of islands. During

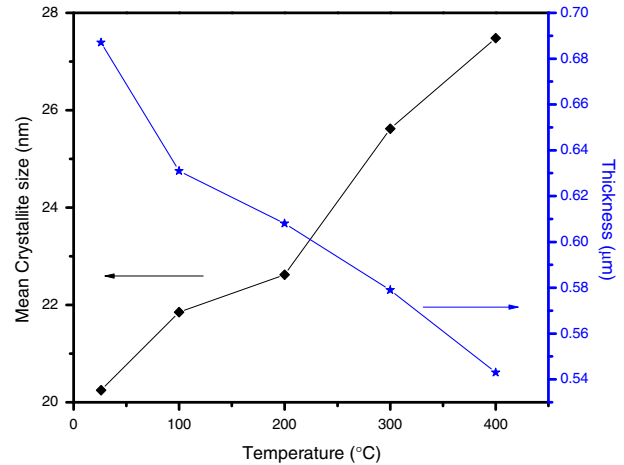


**Figure 3.** Variation of mean crystallite size and film thickness with annealing temperature.

the deposition, smaller crystallites are formed. But on post-deposition annealing, sufficient thermal energy is available for the grains to accelerate the coalescence process to form larger crystallites [20]. Also the crystallites utilize the thermal energy to orient in proper equilibrium sites giving more preferentially oriented films. The variation of crystallite size corresponding to (0 0 2) peak calculated using Scherrer formula is shown in figure 3.

The defects in the films can be quantified by computing the dislocation density ( $\delta$ ) which is defined as the length of dislocation lines per unit volume of the crystal [21]. For preferential orientation, it was calculated using the formula given below [22]:

$$\delta = \frac{1}{D^2} \quad (2)$$

and the values are given in table 2.

The lattice parameters for the hexagonal structure ( $a = b$ ) can be determined using the relation [23]

$$\frac{1}{d_{(hkl)}^2} = \frac{4}{3} \left[ \frac{h^2 + hk + k^2}{a^2} \right] + \frac{l^2}{c^2}. \quad (3)$$

For the (0 0 2) orientation, the lattice parameters are given by

$$a = \frac{\lambda}{\sqrt{3} \sin \theta} \quad (4)$$

and

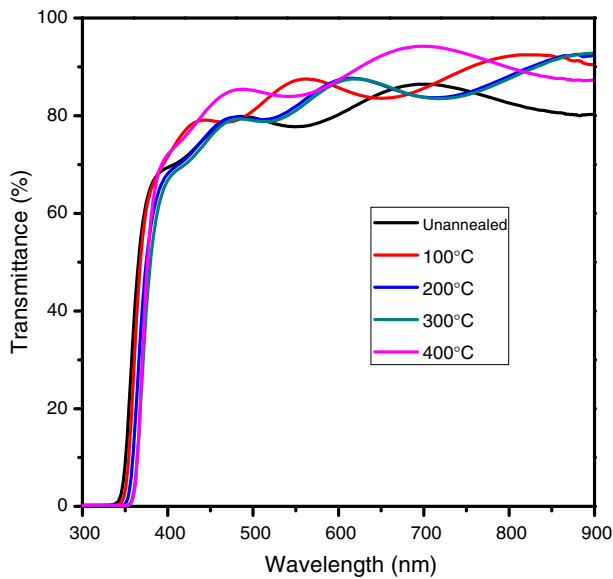
$$c = \frac{\lambda}{\sin \theta}. \quad (5)$$

The unit cell volume can be determined using the expression [23]

$$V = \frac{\sqrt{3}}{2} a^2 c. \quad (6)$$

**Table 2.** Variation of dislocation density ( $\delta$ ), lattice parameters ( $a$  and  $c$ ) and unit cell volume ( $V$ ) for the unannealed and annealed samples.

Temperature (°C)	$\delta$ ( $\times 10^{15} \text{ m}^{-2}$ )	Lattice parameters (nm)		$V$ ( $\times 10^{-30} \text{ m}^3$ )
		$a$	$c$	
Unannealed	2.4386	0.29776	0.51574	39.5984
100	2.0945	0.29764	0.51552	39.5488
200	1.9544	0.29738	0.51508	39.4465
300	1.5235	0.29718	0.51473	39.3676
400	1.3242	0.29678	0.51405	39.2104

**Figure 4.** Transmittance spectra of the unannealed and vacuum-annealed samples of  $\text{Zn}_{0.75}\text{Mg}_{0.25}\text{O}$  thin films.

The calculated values of the lattice parameters and unit cell volume are summarized in table 2. The lattice constants for the unannealed sample are much smaller than that for pure ZnO. This is because the ionic radius of  $\text{Mg}^{2+}$  ion (57 pm) is smaller than that of  $\text{Zn}^{2+}$  ion (60 pm). With annealing, the lattice parameters and unit cell volume further decreased due to the removal of void spaces in the lattice and hence unit cells will be closely packed.

### 3.2 Optical studies

Figure 4 shows the optical transmittance spectra of the unannealed and vacuum-annealed thin films of  $\text{Zn}_{0.75}\text{Mg}_{0.25}\text{O}$  alloy recorded in the 300–900 nm wavelength range. All the films showed better optical transmittance in the visible region and a sharp absorption edge in the near-ultraviolet region. With increase in annealing temperature, the transmittance was improved and the fundamental absorption edge

corresponding to interband electronic transitions showed a red-shift. The enhancement of optical transmittance with increase in annealing temperature is attributed to the reduction in scattering of photons by grain boundaries and other defects because annealing improves crystallinity and removes defects [24].

The thickness and refractive index ( $n$ ) of the deposited films were calculated using Swanepoel's [25] method. According to Swanepoel, the refractive index of the film

$$n = [N_1 + (N_1^2 - n_s^2)^{1/2}]^{1/2}, \quad (7)$$

where

$$N_1 = \frac{n_s^2 + 1}{2} + \frac{2n_s}{T_m} \quad (8)$$

for the transparent region and

$$N_1 = \frac{n_s^2 + 1}{2} + 2n_s \frac{T_M - T_m}{T_M T_m} \quad (9)$$

for the weak and medium absorbing regions. Here  $n_s$  is the refractive index of the substrate and  $T_M$  and  $T_m$  are the transmission maximum and the corresponding minimum at a certain wavelength  $\lambda$ . The film thickness was calculated using the relation

$$t = \frac{\lambda_1 \lambda_2}{2(\lambda_1 n_2 - \lambda_2 n_1)}, \quad (10)$$

where  $n_1$  and  $n_2$  are the refractive indices at two adjacent maxima (minima) and  $\lambda_1$  and  $\lambda_2$  are the corresponding wavelengths. All the calculated values are presented in table 3. The thickness was found to decrease with increase in annealing temperature. This might be due to the availability of sufficient thermal energy to closely pack the unit cells and reconstruct the lattice into denser films. The variation of film thickness with annealing temperature is shown in figure 3.

Band gap energy ( $E_g$ ) of the deposited  $\text{Zn}_{0.75}\text{Mg}_{0.25}\text{O}$  thin films were calculated using the Tauc relation [26]

$$\alpha = \frac{B}{h\nu} (h\nu - E_g)^n, \quad (11)$$

**Table 3.** Variation of thickness ( $t$ ) and energy gap ( $E_g$ ) for the unannealed and annealed samples.

Temperature (°C)	$t$ ( $\mu\text{m}$ )	$E_g$ (eV)
Unannealed	0.687	3.529
100	0.631	3.505
200	0.608	3.476
300	0.579	3.424
400	0.543	3.405

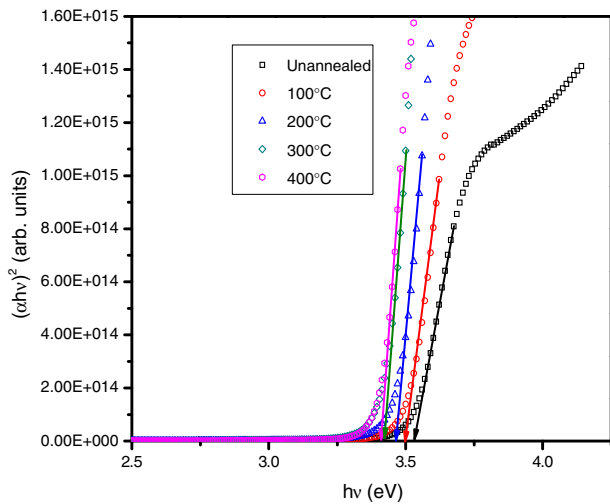


**Figure 5.** Evolution of  $(\alpha hv)^2$  vs.  $h\nu$  curves of the unannealed and annealed thin films of  $\text{Zn}_{0.75}\text{Mg}_{0.25}\text{O}$  alloy.

where  $h\nu$  is the photon energy,  $B$  is the slope of the Tauc edge called the band tailing parameter and  $n$  is a constant equal to  $1/2$  for direct gap materials and  $2$  for indirect transitions. The  $(\alpha hv)^2$  vs.  $(h\nu)$  plots for the films are presented in figure 5. From the linearity of the plots near the absorption edge, it was confirmed that all the films possessed direct optical gap and were obtained as the intercepts on the energy axis by extrapolating the linear portion of the graph.

The energy gap value is found to decrease with increase in annealing temperature and its variation is shown in figure 6. The band-gap values estimated from the Tauc plot for the cation-substituted samples were a little higher than that of pure ZnO thin films reported in the literature [27–29]. The increase in the optical energy gap value with  $\text{Mg}^{2+}$  ion incorporation is attributed to the electronic perturbation caused by cation substitution. The observed red-shift in band gap with increase in annealing temperature could be attributed to the reduction in the polycrystalline nature and hence to the decrease in quantum size effect. In the present case, the mean crystallite size increases and

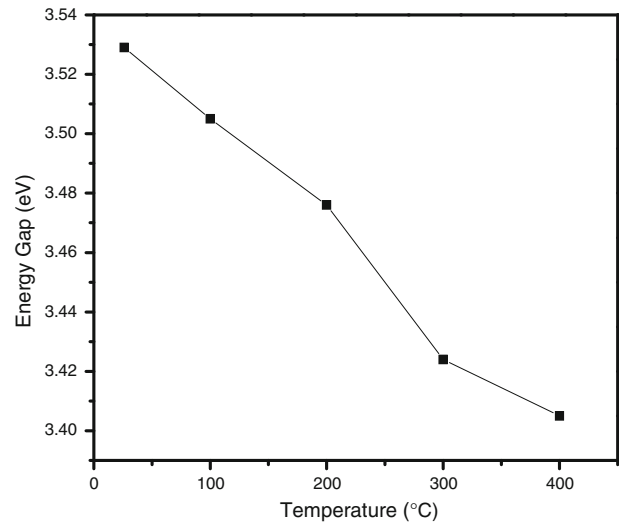


**Figure 6.** Variation of energy gap ( $E_g$ ) with annealing temperature.

causes a reduction in quantum size effect. As can be seen from the X-ray diffractograph, vacuum annealing induces an improvement in crystalline quality because thermal energy accelerates the growth of larger crystallites in preferred direction and reduces band gap for annealed films.

#### 4. Conclusions

$\text{Zn}_{0.75}\text{Mg}_{0.25}\text{O}$  thin films were prepared by sol–gel dip coating method. The XRD patterns of the unannealed and annealed samples reveal the polycrystalline nature of the films with hexagonal wurtzite structure. Because of the successful incorporation of  $\text{Mg}^{2+}$  either at the  $\text{Zn}^{2+}$  lattice site or at the interstitial positions, there is no additional phase corresponding to MgO. XRD pattern shows a slight shift of diffraction angle corresponding to the (0 0 2) peak towards higher values due to the contraction suffered by the lattice accompanied with thermal annealing by way of the removal of defects and disorders. The mean crystallite size for the (0 0 2) peak is found to increase with increasing temperature. This is because, sufficient thermal energy becomes available for grains to accelerate the coalescence process to form larger crystallites. The enhancement of optical transmittance with annealing temperature is attributed to the reduction in scattering of photons by grain boundaries and other defects. The energy gap value of the  $\text{Mg}^{2+}$ -substituted ZnO thin films is higher than that of pure ZnO thin films and is found to decrease with annealing temperature. The

observed red-shift in band gap is due to the improvement in crystallinity and the consequent decrease in quantum size effect.

### Acknowledgements

One of the authors, Nripasree Narayanan, would like to gratefully acknowledge University Grants Commission (UGC), New Delhi, India for providing Junior Research Fellowship (JRF).

### References

- [1] N F Cooray, K Kushiya, A Fujimaki, D Okumura, M Sato, M Ooshita and O Yamase, *Jpn J. Appl. Phys.* **38**, 6213 (1999)
- [2] C Liewhiran and S Phanichphant, *Sensors* **7**, 1159 (2007)
- [3] J Gao, A J Heeger, J Y Lee and C Y Kim, *Synth. Met.* **82**, 221 (1996)
- [4] B J Norris, J Anderson, J F Wager and D A Keszler, *J. Phys. D: Appl. Phys.* **36**, L105 (2003)
- [5] R Paneva and D Gotchev, *Sens. Actuat. A: Phys.* **72**, 79 (1999)
- [6] S J Pearton, D P Norton, K Ip, Y W Heo and T Steiner, *Prog. Mater. Sci.* **50**, 293 (2005)
- [7] A Ohtomo, M Kawasaki, T Koida, K Masubuchi, H Koinuma, Y Sakurai, Y Yoshida and Y Segawa, *Appl. Phys. Lett.* **72**, 2466 (1998)
- [8] Y J Lin, P H Wu, T L Tsai, C J Liu, Z R Lin, H C Chang and C T Lee, *J. Appl. Phys.* **100**, 003701 (2006)
- [9] K Matsubara, H Tampo, H Shibata, A Yamada, P Fons, K Iwata and S Niki, *Appl. Phys. Lett.* **85**, 1374 (2004)
- [10] K P Misra, R K Shukla, A Srivastava and A Srivastava, *Appl. Phys. Lett.* **95**, 031901 (2009)
- [11] V Lujala, J Skarp, T Tamenmaa and T Suntola, *Appl. Surf. Sci.* **82/83**, 34 (1994)
- [12] M-Y Han and J-H Jou, *Thin Solid Films* **260**, 58 (1995)
- [13] U Griebner, R A Kaindl, T Elsaesser and W Seeber, *Appl. Phys. B* **67**, 75 (1998)
- [14] T Mizuta, T Ishibashi, T Minemoto, H Takakura and Y Hamakawa, *Thin Solid Films* **515**, 2458 (2006)
- [15] Y-S Kim, W-P Tai and S-J Shu, *Thin Solid Films* **491**, 153 (2005)
- [16] M Purica, E Budianu, E Rusu, M Danila and R Gavrilă, *Thin Solid Films* **485**, 403 (2002)
- [17] J D Pedarnig, M Peruzzi, I Vrejoiu, D G Matei, M Dinescu and D Bäuerle, *Appl. Phys. A* **81**, 339 (2005)
- [18] S Yang, Y Liu, Y Zheng and D Mo, *Bull. Mater. Sci.* **33(3)**, 209 (2010)
- [19] P P Sahay, S Tewari, R K Nath, S Jha and M Shamsuddin, *J. Mater. Sci.* **43**, 4534 (2008)
- [20] S T Tan, X W Sun, X K Zhang, S J Chua, B J Chen and C C Teo, *J. Appl. Phys.* **100**, 033502 (2006)
- [21] K Ravichandran and P Philominathan, *Sol. Energ.* **82**, 1062 (2008)
- [22] V Bilgin, S Kose, F Atay and I Akyuz, *Mater. Chem. Phys.* **94**, 103 (2005)
- [23] C Suryanarayana and M Grant Norton, *X-ray diffraction – A practical approach* (Plenum Press, New York and London, 1998)
- [24] L Znaidi, G J Soler-Illia, S Benyahia, C Sanchez and A V Kanaev, *New J. Chem.* **24**, 493 (2000)
- [25] J C Manificier, J Gasiot and J P Fillard, *J. Phys. E* **9**, 1002 (1976)
- [26] Y Ohta, Y Haga and Y Abe, *Jpn. J. Appl. Phys.* **36**, L1040 (1997)
- [27] J M Khoshman and M E Kordesch, *Thin Solid Films* **515**, 7393 (2007)
- [28] L Zhang, Z Chen, Y Tang and Z Jia, *Thin Solid Films* **492**, 24 (2005)
- [29] T P Rao and M C Santhoshkumar, *Appl. Surf. Sci.* **255**, 4579 (2009)